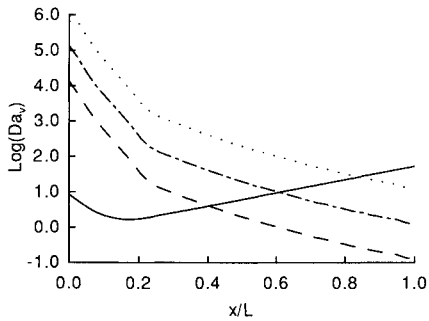

Fig. 4 Axial profiles of vibrational Damköhler number Da_v. Dashed line, p_cL_d = 10 kPa-m; dashed-dotted line, p_cL_d = 100 kPa-m; dotted line, p_cL_d = 1000 kPa-m; solid line, nozzle contour.

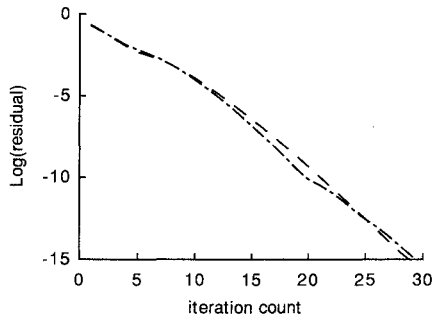

Fig. 5 Decay of the residual of the computation. Dashed-dotted line, perfect gas; dashed line, imperfect gas.

thermal equilibrium is satisfied in most parts of the nozzle but fails in the final part of the divergent section for low values of p_cL_d (i.e., for short nozzles operating at a low stagnation pressure). For $Da_v \ll 1$ the gas behavior is better represented by assuming c_p to be constant. In applications to high-expansion-ratio nozzles a "sudden freezing" model[10,12] can be used to bridge regions computed under the hypotheses of thermal equilibrium (i.e., imperfect gas) and vibrationally frozen flow (perfect gas). The results shown in Fig. 4 are conservative in that the actual rates of vibrational relaxation are faster than assumed here. In typical shock tunnel flows the vibrational relaxation rates are known to be faster than those given by the Landau-Teller model by a factor between 3 and 100 (Ref. 13). When this phenomenon is accounted for, the range of applicability of the present work becomes much wider than that shown in the figure.

Figure 5 compares the convergence history of the computations for a perfect and an imperfect gas. The solution is initialized by prescribing the same (arbitrary) Mach number distribution in both cases. It is apparent that the solution algorithm described in Sec. III gives an extremely fast convergence rate, with the steady state reached in as few as 30 iterations.

V. Conclusions

The proposed formulation demonstrates the possibility of effectively extending all computational techniques developed for the λ formulation to imperfect gas flows, with minimum coding and computational effort.

References

[1]Moretti, G., "The λ-Scheme," *Computers & Fluids,* Vol. 7, No. 3, 1979, pp. 191–205.

[2]Moretti, G., "An Efficient Euler Solver, with Many Applications," AIAA Paper 87-0352, Jan. 1987.

[3]Lentini, D., and Onofri, M., "Solutore Numerico Veloce per Flussi Chimicamente Reagenti in Nonequilibrio," *L'Aerotecnica Missili e Spazio,* Vol. 65, No. 3, Sept. 1986, pp. 110–118.

[4]Lentini, D., and Onofri M., "Nonequilibrium Chemically Reacting Flows in Nozzles," *Analysis and Design of Advanced Energy Systems: Fundamentals,* Vol. 3-1, edited by M. J. Moran and R. A. Gaggioli, American Society of Mechanical Engineers, AES, New York, 1987, pp. 33–40.

[5]Lentini, D., and Onofri, M., "Fast Numerical Technique for Nozzle Flows with Finite-Rate Chemical Kinetics," *Computational Fluid Dynamics,* Proceedings II International Symposium on Computational Fluid Dynamics, North-Holland, Amsterdam, 1988, pp. 449–460.

[6]Moretti, G., and Zannetti, L., "A New, Improved Computational Technique for Two-Dimensional Unsteady Compressible Flows," AIAA Paper 82-0168, Jan. 1982.

[7]Moretti, G., "A Fast Euler Solver for One-Dimensional Flows," NASA CR 3689, June 1983.

[8]"Table of Coefficient Sets for NASA Polynomials," *Combustion Chemistry,* edited by W. C. Gardiner, Springer-Verlag, New York, 1984, pp. 485–504.

[9]Reynolds, W. C., "The Element Potential Method for Chemical Equilibrium Analysis: Implementation in the Interactive Program STANJAN," Dept. of Mechanical Engineering, Stanford Univ., Stanford, CA, Jan. 1986.

[10]Bray, K. N. C., "Chemical and Vibrational Nonequilibrium in Nozzle Flows," *Nonequilibrium Flows,* Vol. 1, Part II, edited by P. P. Wegener, Dekker, New York, 1970, pp. 70–75, 93–98.

[11]Vincenti, W. G., and Kruger, C. H., *Introduction to Physical Gas Dynamics,* Wiley, New York, 1965, pp. 198–206.

[12]Phinney, R., "Criterion for Vibrational Freezing in a Nozzle Expansion," *AIAA Journal,* Vol. 1, No. 2, 1963, pp. 496–497.

[13]Hurle, I. R., "Nonequilibrium Flows with Special Reference to the Nozzle-Flow Problem," *Proceedings of the 8th International Shock Tube Symposium,* Chapman and Hall, London, 1971, pp. 3/1–3/37.

Surface Reaction Model for Catalyzed Composite Solid Propellants

S. Krishnan* and R. Jeenu†
Indian Institute of Technology, Madras 60036, India

Nomenclature

A = kinetic pre-exponential factor
A_{fc} = oxidizer particle area fraction of the enhanced condensed phase exothermic decomposition
c_p = average specific heat capacity for the solid and gases
D_0 = oxidizer particle diameter
E = activation energy
K = constant dependent on type of catalyst and surface/subsurface reaction
m = mass flux
Q = heat release
R = universal gas constant
S = surface area
T = temperature
α = mass fraction of ingredient in propellant
β_F = fraction of oxidizer that partake in primary flame reaction
Γ = catalyst specific surface dependent constant
ϵ = ratio of oxidizer decomposed due to a condensed phase exothermic decomposition to the total oxidizer decomposed
λ = thermal conductivity
Φ = stoichiometric oxidizer/fuel ratio
ρ = density
ξ^* = dimensionless flame height

Received March 9, 1991; revision received Jan. 2, 1992; accepted for publication Jan. 22, 1992.

*Professor, Department of Aerospace Engineering. Senior Member AIAA.

†Research Associate, Department of Aerospace Engineering.

Ω = catalyst mass concentration in binder multiplied by catalyst specific surface area

Subscripts

AP = associated with oxidizer monopropellant flame
c = catalyzed condition
FF = associated with final flame
f = binder or referring to binder characteristics
ox = oxidizer or referring to oxidizer
P = planar
PDF = associated with total primary flame
r = limit above which interfacial reaction is possible
s = surface
ss = subsurface
T = total
0 = initial condition or total surface
1 = associated with condensed phase exothermic decomposition
2 = associated with oxidizer sublimation

Introduction

THE two extensions suggested so far to the well-known Beckstead, Derr, and Price (BDP) model[1] to account for catalytic effect, one by Cohen[2] and the other by Beckstead,[3] do not adequately predict the burning rate variations; the former works well at high pressures (10–100 bar), whereas the latter is effective only at low pressures (0.03–1 bar). In addition, contrary to experimental results,[4-6] the model and its extensions are insensitive to oxidizer particle size variation at subatmospheric and near-atmospheric pressures. This is due to the constant surface heat release assumption. Experimental studies[5,7] indicate that this heat release is not constant but varies with pressure, oxidizer particle size, and catalytic concentration; therefore, the present study incorporates a variable surface and subsurface heat release into the BDP model and shows that the model can successfully predict the effects of catalysts and oxidizer particle size at low as well as rocket operating pressures. Extending the validity of the model to low pressures will be useful in predicting the early stages of ignition transient of rocket motors as well as in the development of propellants for stop-start and missile base bleed motors.

Surface Reaction

There is evidence to believe that ammonium perchlorate (AP) can decompose in parallel condensed phase exothermic decomposition (CPED) and sublimation, and the former may lead to AP/binder interfacial heterogeneous reactions. Regarding the AP decomposition, Powling[8] proposes that a significant degree of CPED to Cl_2, O_2, H_2O, and N_2O may accompany sublimation to NH_3 and $HClO_4$; the Cl_2 and O_2 from CPED may combine with adjacent fuel elements through heterogeneous reaction. At low pressures, the gas phase combustion zone thickness in composite propellant flame is large; therefore, the heat feedback from gas phase is less. On the other hand, due to the deeper high-temperature penetration and, hence, the longer residence time allotted for the reactions at and beneath the surface, surface-subsurface reactions take a dominant role in maintaining the necessary surface temperature. The flameless combustion of uncatalyzed AP/polysulphide propellants at low pressures[6,9] and the crevices found around AP particles in extinguished composite propellants [Ref. 10 (7 bar), Ref. 5 ($\leq$41 bar)] support this proposition.

Numerous thermal analyses of AP/catalyst systems suggest that catalysts increase considerably the extent of CPED.[8] Low pressure studies on AP/hydroxyl-terminated polybutadiene (HTPB) propellants[5,6] demonstrate the following: 1) the addition of Fe_2O_3 leads to the flameless combustion condition, and that of copper chromite catalyst to the presence of thick dark zone—both point out negligible gas phase heat feedback to the surface; and 2) the presence of catalysts reduces the burning rate pressure exponent with significant burning rate enhancements existing down to the lowest burning pressure. With regard to the mechanism of burning rate enhancement, we may consider the physical situation of catalyst particles in the propellant microstructure as follows. With the advancement of flame front, the catalyst particles may decompose, evaporate, leave the surface, or adhere to the receding surface. Price and Sambamurthi[11] demonstrate the last possibility through their studies on AP/polybutadiene-acrylic acid-acrylonitrile (PBAN)/Fe_2O_3 propellants. Although the adhering catalyst particles are generally more favorably positioned to affect binder decomposition, Cohen et al.[12] conclude that catalysts do not manifest themselves by direct influence upon binder pyrolysis. Jones and Strahle[13] observe that catalysts do not promote heterogeneous reactions of gases with the binder, or modify its pyrolysis mechanism, but possibly promote gas phase or heterogeneous reactions at the AP/binder interface. These adhering catalyst particles will of course encounter emerging oxidizer crystals and may get blown off by the oxidizer decomposition products but for a possible catalytic effect at the oxidizer particle peripheral areas. According to Logachev et al.,[14] the important feature of catalytic mechanism is the contact of the catalyst particles with AP and the diffusion of ClO_4^- to catalyst. Scanning electron micrographs[5,11] reveal that the addition of catalysts affects the peripheral but not central areas of coarse AP particles. Thus, it is possible that with catalysts the burning rate controlling reactions are located in the condensed phase; the catalyst may enhance the CPED at the AP particle peripheral areas, and consequently enhance AP/binder interfacial heterogeneous reactions.

Governing Equations

At the surface, $m_{ox,s,c}$ is assumed to be the sum of the uncatalyzed rate and the rate due to catalytic effect—both of zero-order reaction. The effects of catalysts on the kinetics pre-exponential factor and activiation energy are not clearly understood. However, it is assumed that the addition of a catalyst affects only the pre-exponential factor.[2] Hence,

$$m_{ox,s,c} = A_{ox,s}[1 + A_{fc}K_{ox,s}\Omega/(\Gamma + \Omega)]\exp[-E_{ox,s}/(RT_s)] \quad (1)$$

where Γ is selected to give the diminishing return in burning rate enhancement with increase in concentration.[3] The AP fraction that reacts by the CPED under catalyzed condition can be written as

$$\epsilon_c = \{\epsilon[1 + K_{ox,s,1}\Omega/(\Gamma + \Omega)]\}/[1 + \epsilon K_{ox,s,1}\Omega/(\Gamma + \Omega)] \quad (2)$$

Thus,

$$Q_{ox} = (1 - A_{fc})[\epsilon Q_{ox,1} + (1 - \epsilon)Q_{ox,2}] + A_{fc}[\epsilon_c Q_{ox,1} + (1 - \epsilon_c)Q_{ox,2}] \quad (3)$$

In the subsurface, for the uncoupled subsurface temperature profile, the oxidizer reacted under catalyzed condition at the oxidizer/binder interface per unit propellant planar area,

$$m_{ox,ss,c} = \{3\pi/[2D_o(1 + [(1 - \alpha_{ox})/\alpha_{ox}]\rho_{ox}/\rho_f)\}[\lambda/(m_T c_p)] A_{ox,ss}[1 + K_{ox,ss}\Omega/(\Gamma + \Omega)] \int_{T_r}^{T_s} \exp[-E_{ox,ss}/(RT)]\, dT/(T - T_0) \quad (4)$$

Taking overall mass balance at the propellant surface,

$$m_T S_o = (m_{ox,s} S_{ox,s} + m_{ox,ss} S_P)/\alpha_{ox} = (m_{f,s}S_{f,s} + m_{ox,ss}S_P)/\Phi)/(1 - \alpha_{ox}) \quad (5)$$

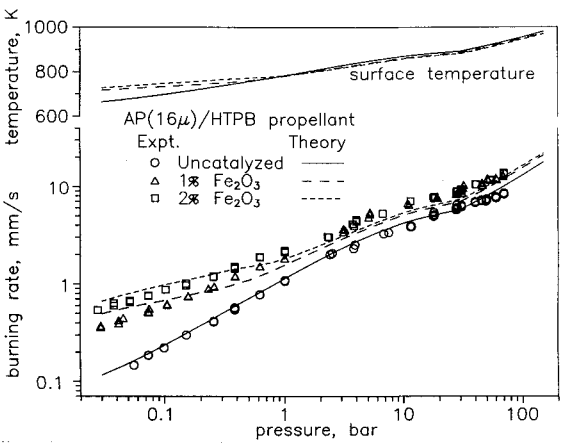

Fig. 1 Comparison of theory with experiment[5] and effect of catalyst concentration.

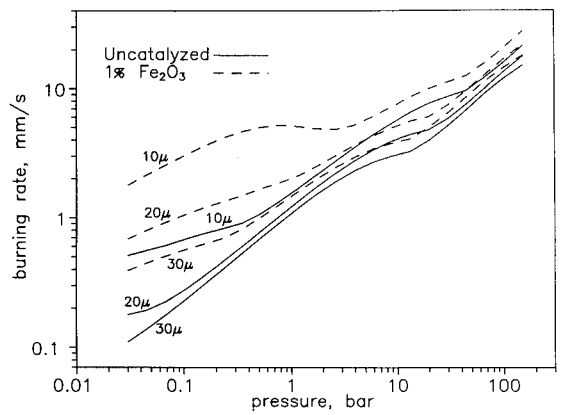

Fig. 2 Effect of AP particle size and catalyst concentration on burning rate—computer propellant of AP/HTPB (73/27).

The following energy consideration gives Q_{PDF}:

$$[(m_{ox,s}S_{ox,s} + m_{f,s}S_{f,s})\beta_F + m_{ox,ss}(1 + 1/\Phi)S_P]Q_{\text{PDF}}$$
$$= [(m_{ox,s}S_{ox,s} + m_{f,s}S_{f,s})\beta_F$$
$$+ m_{ox,ss}(1 + 1/\Phi)S_P]c_p(T_{\text{PDF}} - T_0) + m_{ox,s}S_{ox,s}\beta_F Q_{ox}$$
$$+ m_{f,s}S_{f,s}\beta_F Q_f + m_{ox,ss}(1 + 1/\Phi)S_P Q_{ss} \quad (6)$$

In the gas phase, the other heat release equations are same as in Ref. 1. Now, the averaged surface temperature can be obtained from the following revised energy conservation equation.

$$m_T c_p(T_s - T_0) = -m_{ox,ss}(1 + 1/\Phi)(S_P/S_0)Q_{ss}$$
$$- m_{ox,s}(S_{ox,s}/S_0)Q_{ox} - m_{f,s}(S_{f,s}/S_0)Q_f$$
$$+ \{\beta_F[m_{ox,s}(S_{ox,s}/S_0) + m_{f,s}(S_{f,s}/S_0)]$$
$$+ m_{ox,ss}(1 + 1/\Phi)(S_P/S_0)\}Q_{\text{PDF}}\exp(-\xi^*_{\text{PDF}})$$
$$+ (1 - \beta_F)m_{ox,s}(S_{ox,s}/S_0)[Q_{\text{AP}}\exp(-\xi^*_{\text{AP}})$$
$$+ Q_{FF}\exp(-\xi^*_{FF})]$$

Results

$E_{ox,ss}$ is taken as 32.5 kcal/mole,[15] and the value $A_{ox,ss}$ of 10^8 g/cm^2 · s is chosen such that the low-pressure burning rate fitting for uncatalyzed propellant is satisfactory. Noting from the thermal decomposition studies that AP starts to decompose at 200°C and the decomposition goes to 100% between 250–350°C, an approximate average value of 550 K for T_r seems to be reasonable. ϵ is taken as 0.5, and this implies that the maximum possible available energy from the monopropellant AP flame (~ 810 cal/g) is equally shared by the monopropellant gas phase flame and CPED. In the absence of any detailed information, the extent of A_{fc} is taken as that corresponding to 1 μm peripheral width. Taking other data from Ref. 16, the principal equations (1), (4), (5), and (7) are solved for a range of pressures. Figure 1 shows the typical experimental data[5] and the curves predicted by the present study. The results of calculations for computer propellants of different particle size and catalytic concentrations are given in Fig. 2. The predicted burning rates are now in much better agreement with the general experimental observations: 1) the burning rate increases with diminishing returns with increase in catalyst concentration, and 2) both particle size effectiveness and catalytic effectiveness on burning rate are positive from the lowest burning pressure to the rocket operating pressure and these generally increase with decrease in pressure.

Acknowledgment

The present work forms a part of the research sponsored by the Department of Space, Government of India, under Sanction 9/1(5)/87-II.

References

[1]Beckstead, M. W., Derr, R. L., and Price, C. F., "A Model of Composite Solid-Propellant Combustion Based on Multiple Flames," *AIAA Journal*, Vol. 8, No. 12, 1970, pp. 2200–2207.

[2]Cohen, N. S., "Review of Composite Propellant Burn Rate Modeling," *AIAA Journal*, Vol. 18, No. 3, 1980, pp. 277–293.

[3]Beckstead, M. W., "A Model for Solid Propellant Combustion," *Proceedings of 14th JANNAF Combustion Meeting*, CPIA Pub. 292, Johns Hopkins Univ., Baltimore, MD, Vol. I, Dec. 1977, pp. 281–306.

[4]Kishore, K., "Comprehensive View of the Combustion Models of Composite Solid Propellants," *AIAA Journal*, Vol. 17, No. 11, 1979, pp. 1216–1224.

[5]Kishnan, S., and Jeenu, R., "Combustion Characteristics of AP/HTPB Propellants with Burning Rate Modifiers," *Journal of Propulsion and Power* (to be published).

[6]Steinz, J. A., and Summerfield, M., "Low Pressure Burning of Composite Solid Propellants," *Propellant Manufacture, Hazards and Testing*, edited by R. F. Gould, Advances in Chemistry Series, No. 88, American Chemical Society, Washington, DC, 1969, pp. 244–295.

[7]Waesche, R. H. W., Wenograd, J., and Feinaner, L. R., "Investigations of Solid-Propellant Decomposition Characteristics and Their Relations to the Observed Burning Rates," ICRPG/AIAA Second Solid Propulsion Conference, June 1967.

[8]Powling, J., "Experiments Relating to the Combustion of Ammonium Perchlorate-Based Propellants," *Eleventh Symposium (International) on Combustion*, Combustion Inst., Pittsburgh, PA, 1967, pp. 447–456.

[9]Wenograd, J., Comment on "The Surface Temperature of Ammonium Perchlorate Burning at Elevated Pressures" by J. Powling and W. A. W. Smith, *Tenth Symposium (International) on Combustion*, Combustion Inst., Pittsburgh, PA, 1965, pp. 1379–1380.

[10]Boggs, T. L., Derr, R. L., and Beckstead, M. W., "Surface Structure of Ammonium Perchlorate Composite Propellants," *AIAA Journal*, Vol. 8, No. 2, 1970, pp. 370–372.

[11]Price, E. W., and Sambamurthi, J. K., "Mechanism of Burn Rate Enhancement by Ferric Oxide," Chemical Propulsion Information Agency, CPIA Publ. 412, Johns Hopkins Univ., Baltimore, MD, Vol. 1, 1984.

[12]Cohen, N. S., Fleming, R. W., and Derr, R. L., "Role of Binders in Solid Propellant Combustion," *AIAA Journal*, Vol. 12, No. 2, 1974, pp. 212–218.

[13]Jones, H. E., and Strahle, W. C., "Effects of Copper Chromite and Iron Oxide Catalysts on AP/CTPB Sandwiches," *Fourteenth Symposium (International) on Combustion*, Combustion Inst., Pittsburgh, PA, 1972, pp. 1287–1295.

[14]Logachev, V. S., Dmitriev,. A. S., and Pokhil, P. F., "Mechanism of Action of Catalysts on Ammonium Perchlorate," *Doklady Academii Nauk SSSR*, Vol. 214, May 1974, pp. 1113–1116; *Chemical Abstracts*, Vol. 81, 1974, p. 54760.

[15]Hermance, C. E., "A Model of Composite Propellant Combustion Including Surface Heterogeneity and Heat Generation," *AIAA Journal*, Vol. 4, No. 9, 1966, pp. 1629-1637.

[16]Ramohalli, K. N. R., "Steady-State Burning of Composite Propellants under Zero Cross-Flow Situation," *Fundamentals of Solid-Propellant Combustion*, edited by K. K. Kuo and M. Summerfield, Vol. 90, Progress in Astronautics and Aeronautics, AIAA, New York, 1984, pp. 409-477.

Stiffness Design Method of Symmetric Laminates Using Lamination Parameters

Hisao Fukunaga* and Hideki Sekine
Tohoku University, Sendai 980, Japan

Introduction

IN the stiffness design of laminated composites, it is important to optimize layer angles as well as layer thicknesses. Introducing lamination parameters as design variables is efficient and reliable in the optimization of laminated composites since the stiffness components of laminated composites are expressed as a linear function with respect to lamination parameters.[1] To use lamination parameters in the design of laminated composites, the feasible region of lamination parameters needs to be known. The method for determining the laminate configurations corresponding to the lamination parameters also has to be established. The previous paper[2] has shown those fundamental relations for a specially orthotropic laminate eliminating coupling terms.

In the symmetric laminate with the extension-shear coupling or the bending-twisting coupling, the in-plane and out-of-plane stiffness characteristics are governed by four in-plane and four out-of-plane lamination parameters, respectively. The present paper shows the feasible region of in-plane or out-of-plane lamination parameters for the symmetric laminate. A method is proposed for determining laminate configurations corresponding to the lamination parameters.

Stiffness Characteristics of Symmetric Laminates

In the classical lamination theory, the constitutive equation of symmetric laminates is given by

$$\begin{Bmatrix} N \\ M \end{Bmatrix} = \begin{pmatrix} A & 0 \\ 0 & D \end{pmatrix} \begin{Bmatrix} \epsilon \\ \kappa \end{Bmatrix} \tag{1}$$

where N and M denote the stress and moment resultants, respectively; ϵ and κ denote the strains and the curvature changes at the midplane, respectively; and A_{ij} and D_{ij} represent the in-plane and the out-of-plane stiffnesses, respectively.

When the stiffness components A_{ij} and D_{ij} $(i,j=1,2,6)$ are expressed by the stiffness invariants and the lamination parameters,[1] A_{ij} and D_{ij} are governed by four in-plane and four out-of-plane lamination parameters, respectively,

$$\xi_1 = \int_0^1 \cos 2\theta(u)\, du, \quad \xi_2 = \int_0^1 \cos 4\theta(u)\, du$$
$$\xi_3 = \int_0^1 \sin 2\theta(u)\, du, \quad \xi_4 = \int_0^1 \sin 4\theta(u)\, du \tag{2}$$

$$\xi_9 = 3\int_0^1 \cos 2\theta(u)u^2\, du, \quad \xi_{10} = 3\int_0^1 \cos 4\theta(u)u^2\, du$$
$$\xi_{11} = 3\int_0^1 \sin 2\theta(u)u^2\, du, \quad \xi_{12} = 3\int_0^1 \sin 4\theta(u)u^2\, du \tag{3}$$

where $\theta(u)$ is a distribution function of the fiber angles through the thickness, and $(\xi_1, \xi_2, \xi_3, \xi_4)$ and $(\xi_9, \xi_{10}, \xi_{11}, \xi_{12})$ represent the in-plane and out-of-plane lamination parameters, respectively. In Eq. (1), the stiffness components are a linear function with respect to the lamination parameters. In the stiffness optimization, the use of lamination parameters as design variables leads to an efficient and reliable optimization approach.

The lamination parameters depend on each other. The relation between the lamination parameters has not been known, although the preceding study was performed in Refs. 3 and 4. The present paper first examines the relation between the four in-plane lamination parameters. As shown in Fig. 1, the feasible region of a point $Q(\xi_2,\xi_4)$ for a fixed point $P(\xi_1, \xi_3)$ is expressed as follows:

$$(\xi_2 - r^2\cos 2\alpha)^2 + (\xi_4 - r^2\sin 2\alpha)^2 \le (1-r^2)^2 \tag{4}$$

where $r\cos\alpha = \xi_1$ and $r\sin\alpha = \xi_3$. Equation (4) is also expressed as follows:

$$\left| \int_0^1 \exp(i4\theta)\, du - \left[\int_0^1 \exp(i2\theta)\, du \right]^2 \right| \le 1 - \left| \int_0^1 \exp(i2\theta)\, du \right|^2 \tag{5}$$

where $|z|$ denotes the absolute value of a complex number z. We can prove the relation of Eq. (5) easily.

When the coupling terms vanish, i.e., $\xi_3 = \xi_4 = 0$, Eq. (4) leads to the following relation:

$$2\xi_1^2 - 1 \le \xi_2 \le 1 \tag{6}$$

Equation (6) gives the feasible region of lamination parameters for the laminate without extension-shear coupling.

Equation (4) shows the feasible region of (ξ_2, ξ_4) for the fixed values of (ξ_1, ξ_3). On the other hand, for the fixed values of (ξ_1, ξ_2), Eq. (4) is transformed as follows:

$$2(1+\xi_2)\xi_3^2 - 4\xi_1\xi_3\xi_4 + \xi_4^2 \le (\xi_2 - 2\xi_1^2 + 1)(1-\xi_2) \tag{7}$$

Equation (7) shows that the feasible region of (ξ_3, ξ_4) is within an ellipse for $1+\xi_2-2\xi_1^2 > 0$ and on the straight line of $\xi_4 = 2\xi_1\xi_3$ $(-1 \le \xi_1 \le 1)$ for $1+\xi_2-2\xi_1^2 = 0$. When the lamination parameters $((\xi_1, \xi_2)$ are specified, the in-plane stiffness components, A_{11}, A_{12}, A_{22}, and A_{66}, are determined uniquely. On the other hand, the extension-shear coupling terms, A_{16}

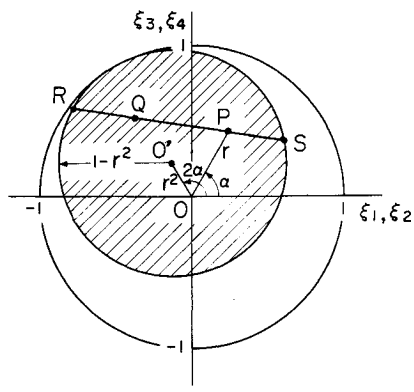

Fig. 1 Feasible region of $Q(\xi_2, \xi_4)$ for $P(\xi_1, \xi_3)$.

Received June 11, 1991; revision received Oct. 10, 1991; accepted for publication Oct. 18, 1991.

*Associate Professor, Department of Aeronautics and Space Engineering, Faculty of Engineering. Member AIAA.

†Professor, Department of Aeronautics and Space Engineering, Faculty of Engineering.